Partial reduction of anthracene by cold field emission in liquid in a microreactor with an integrated planar microstructured electrode

M. Morassutto, P. van der Linde, S. Schlautmann, R.M. Tiggelaar, J.G.E. Gardeniers*

Mesoscale Chemical Systems, MESA⁺ Institute for Nanotechnology, University of Twente, P.O. Box 217, 7500 AE Enschede, The Netherlands

ARTICLE INFO

ABSTRACT

We report a novel microreactor with a photolithographically defined integrated electrode containing micro tips that serve as emission points for solvated electrons into liquid n-hexane in a microfluidic channel. The implementation of sharp electrode tips permits to extract electrons from the electrode material at relatively low voltages. The electric field distribution in the gap between a planar patterned platinum microtip array and a planar rectangular counterelectrode is analyzed by a computational model. Cold field emission using these microdevices is experimentally verified, and the partial reduction of anthracene to 9,10-dihydroanthracene, via solvated electrons emitted in solutions with or without ethanol in n-hexane is investigated. It is found that in the current microreactor configuration, the majority of the products are products originating from coupling of ethanol fragments to, and/or oxidation of 9,10-dihydroanthracene at the platinum counterelectrode, leaving no detectable yield of the desired reduction product.

1. Introduction

Solvated electrons have been observed for the first time in 1807 by Sir Humphry Davy and are mentioned in a scientific report in 1864 by Weyl [1,2]. In more recent days, in particular the nature of the solvated electron in water, the hydrated electron, with its typical characteristics of a short lifetime (nanoseconds), exceptionally high diffusion rate and high reactivity, has been extensively studied [3]. The enormous reducing power of solvated electrons has been noted early on, e.g. in the groundbreaking work of Birch, who investigated the partial reduction of polycyclic aromatic hydrocarbons (PAH) using solvated electrons generated by dissolving an alkali metal in liquid ammonia [4]. More recent studies have focused on the development of greener Birch reduction processes that avoid the use of alkali metals or liquid ammonia, such as electrochemical or plasma techniques [5–7].

Following earlier studies on field emission into organic liquids [8,9], the possibility to generate solvated electrons by cold field emission (CFE) from nanostructured electrodes was proposed by Krivenko et al. and Agiral et al. [10,11]. The latter authors show the possibility to inject electrons directly into liquid hexane by using carbon nanofibers and a defined small interspace between these fibers and a flat counter electrode. The micrometer range electrode gap and the nanometer scale radius of curvature of the structures on the cathode surface facilitate the emission of electrons by creating a high electric field with only a relatively low voltage difference.

State of the art microfabrication technology permits the creation of integrated electrodes with well-defined geometry and dimensions. Using physical vapor deposition (PVD) of a metal film in combination with photolithography, in this report the construction of microreactors, which are suitable to perform CFE in a flow of liquid n-hexane, is described. Background theory of field enhancement is considered and the electrical field distribution around the electrode tips is numerically modeled. Electrical analysis of the electrode configuration is performed, and the chemical performance of the microreactor system for the reduction of anthracene is evaluated.

2. Electrical model and device design aspects

2.1. Microreactor design

The microreactors (Fig. 1) are composed of glass and silicon and have two platinum (Pt) electrodes in a planar configuration positioned at the edges of a flow channel. In order to locally increase the electric field, which enhances the emission of electrons from the metal surface, one of the two electrodes, the cathode, contains lithographically defined microtips with a triangular shape. The distance (d) between the two electrodes is varied within the range: 1, 2, 3, 5, 10 and 20 μm. The cathode consists of a series of isosceles triangles (10 μm height and 10 μm length), connected by a rectangle of 6 mm length and 100 μm width. The thickness of the electrode is 100 nm. The anode is a

---

* Corresponding author.
E-mail address: j.g.e.gardeniers@utwente.nl (J.G.E. Gardeniers).
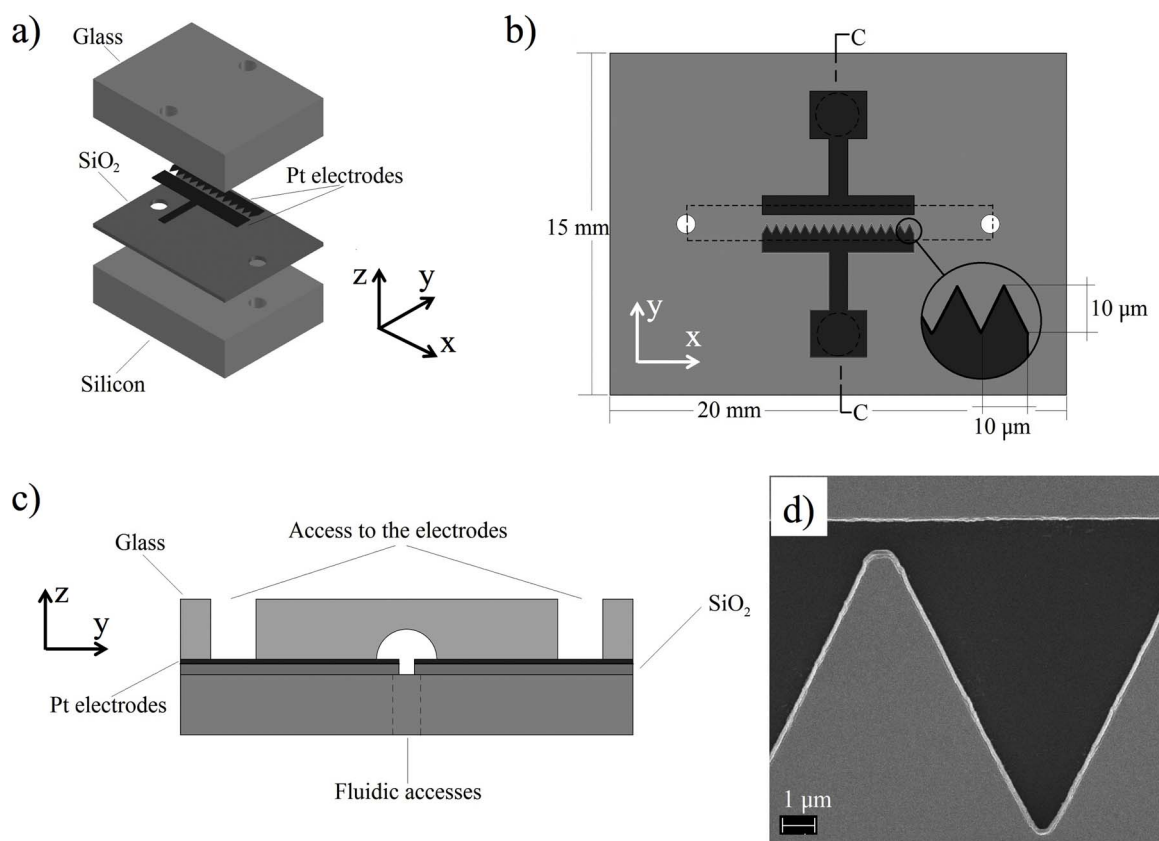
Fig. 1. Microreactor with photolithographically defined microtips: a) 3D exploded view of the microreactor components, b) top view of electrode pattern, c) cross section of microfluidic channel, showing how the electrodes are aligned with the channel, d) SEM image of one of the microtips, for a 1 μm cathode tip to anode distance.

rectangle of 6 mm in length, 100 μm in width and 100 nm thick. Both electrodes are placed at the bottom of the flow channel which is 150 μm wide and 25 μm deep (total reactor volume: 50 nL).

2.2. Electrical field modeling

In order to study the local field enhancement at the microtips, an electrostatic model of the electric field distribution upon applying a potential between the flat anode and the microtips on the cathode surface is created. The model, that was used in the numerical calculations is based on Griffiths' work [12]. The COMSOL 4.3a Multiphysics software package was used to numerically calculate the electrostatic field between an electrode with triangular emitters and a flat counter-electrode, based on the following equations, derived from Gauss' law [13]:

$$E = \nabla V \text{ and } \nabla \varepsilon E = \rho \qquad (1)$$

where ε is the absolute permittivity ($\varepsilon = \varepsilon_r * \varepsilon_0$), E the static electric field, ρ the charge and V the electric potential. The considered dielectric constants (ε_r) in the model are 1 and 2.2 for the platinum electrode and n-hexane, respectively. The model considers the case of a cathode placed at 3 μm from the anode, where the volume between the electrodes is filled with n-hexane. The overall dimension of the model is set at 50 μm width (x-direction), 33 μm depth (y-direction) and 2 μm height (z-direction). These dimensions represent a characteristic part of the microreactor, see Fig. 2.

The mesh for the geometry was set as follows: maximum element size 128 nm, minimum element size 23 nm, maximum element growth rate 1.5, resolution of curvature 0.6 and resolution of the narrow regions 0.5. The initial values of all structures were set to a potential of 0 V, apart from the cathode potential which was set to −4 V. The temperature was set at 293.25 K. The stationary solver was set with its

tolerance at 0.001 and an algebraic multigrid was selected.

3. Materials and methods

3.1. CFE microreactor fabrication

Silicon (100) substrates (p-type boron doped, resistivity 5–10 Ωcm, 100 mm diameter, 525 μm thickness, single side polished; Okmetic, Finland) were cleaned by immersion in fuming 100% nitric acid (UN2031 OM Group) for 10 min, in boiling 69% nitric acid (BASF, 51153574) for 15 min, rinsed in demineralized water, and immersed in 1% aqueous HF (D252 M Honeywell) for 1 min, followed by rinsing in demineralized water and spin drying. 1 μm of SiO_2 was deposited on the substrates in a furnace, using steam oxidation (Tempress, H_2O + N_2 bubbler, N_2 flow 2 L/min, 1150 °C). Electrode structures were photolithographically defined in photoresist (standard UV-lithography, photoresist Olin 907-17). They are centered with respect to a microreactor footprint-size of 20 × 15 mm. In the lithographically defined areas, 150 nm of SiO_2 was removed by immersion in buffered HF solution (BHF; Honeywell, 10188624), followed by rinsing in demineralized water and spin drying. A layer of 100 nm Pt with 10 nm Ta as adhesion layer was sputtered (homemade PVD machine, Ar plasma 200W, $6.66 \cdot 10^{-3}$ mbar, 145 sccm Ar flow rate). After the lift-off process, under ultrasonication in acetone (VLSI 51150924, BASF) for 10 min, the substrates were washed with isopropanol (VLSI 51152037, BASF) followed by rinsing in demineralized water and spin drying. The flow channel of the microreactor (15 mm long with a variable width due to the various electrode spacing) was lithographically defined in photoresist (standard UV-lithography, photoresist Olin 907-17). By means of ion beam etching (15 min IBE etching Oxford i300, current 50 mA, voltage 300 V, generator power 300W) followed by 2.5 min of reactive ion etching (Adixen DE, 20/15/150 sccm flow of $C_4F_8/CH_4/He$,
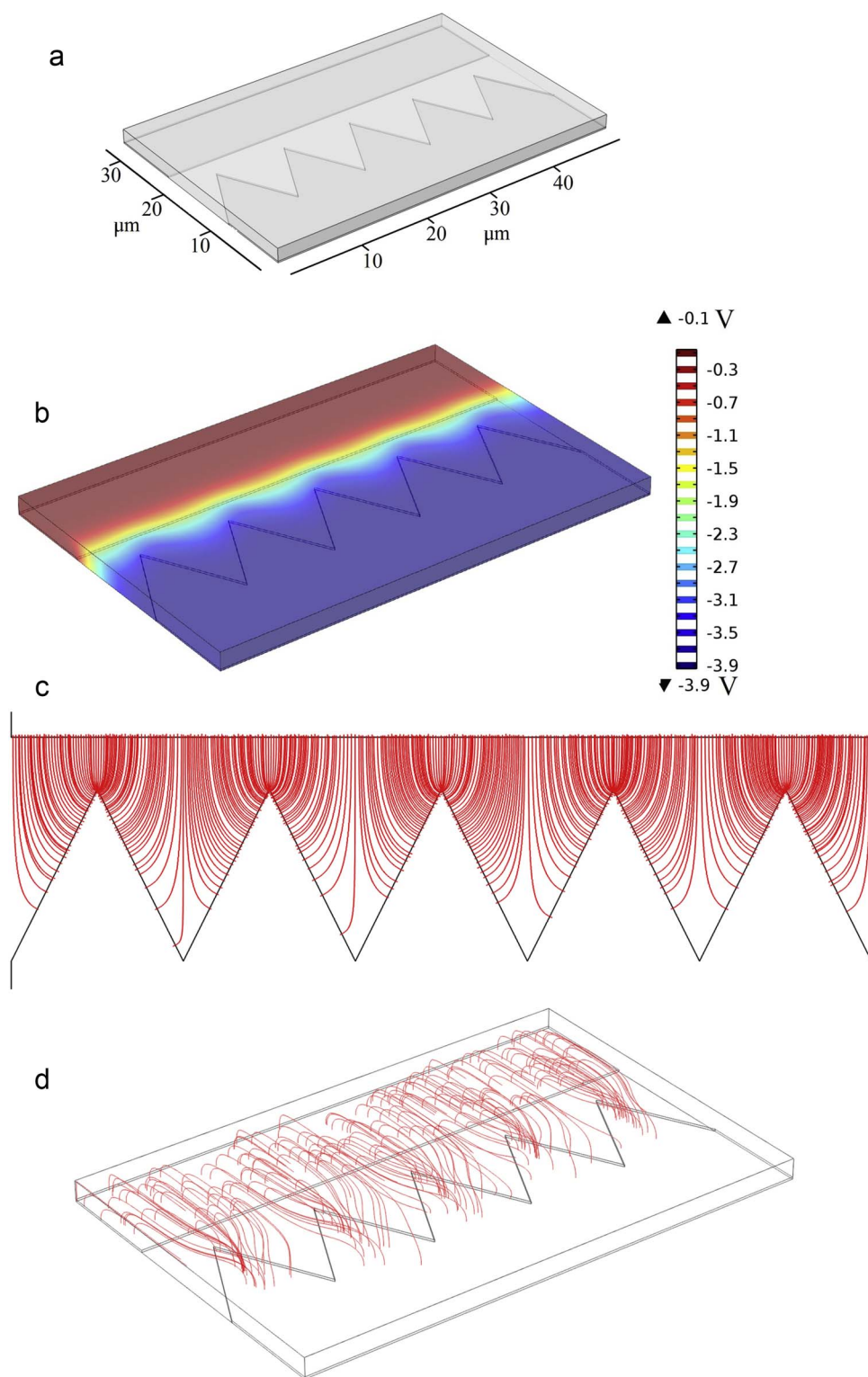
a

b

c

d

8.5 10^{-3} mbar, 2800 W ICP, 350 W CCP) the SiO_2 between the electrodes was removed. On the non-polished backside of the silicon substrate fluidic access holes to the flow channel were created via plasma etching (Adixen SE, T = −40 °C, 175/500 sccm flow rate C_4F_8/SF_6, 2500W ICP, 20W CCP) after standard UV-lithography (photoresist Olin 908-35), after which the remaining photoresist was removed with O_2 plasma (Tepla 300).

On glass substrates (Mempax, 100 mm diameter, thickness 500 μm, Mark Optics, USA), after immersion in fuming 100% nitric acid

(UN2031 OM Group) for 10 min followed by rinsing in demineralized water and spin drying, a layer of 100 nm Au with 10 nm Cr as adhesion layer was sputtered (homemade PVD machine, Ar plasma 200W, $6.66 \cdot 10^{-3}$ mbar, 145 sccm flow rate). This metallic layer served as a masking layer during the fabrication of the flow channel. A 15 mm long straight channel was lithographically defined in photoresist (standard UV-lithography, photoresist Olin 907-17). After ozone exposure (Surf Ozone UV PRS 100 reactor, 300 s.), in order to improve the wetting of the photoresist for proper metal etching, the Au and Cr were removed
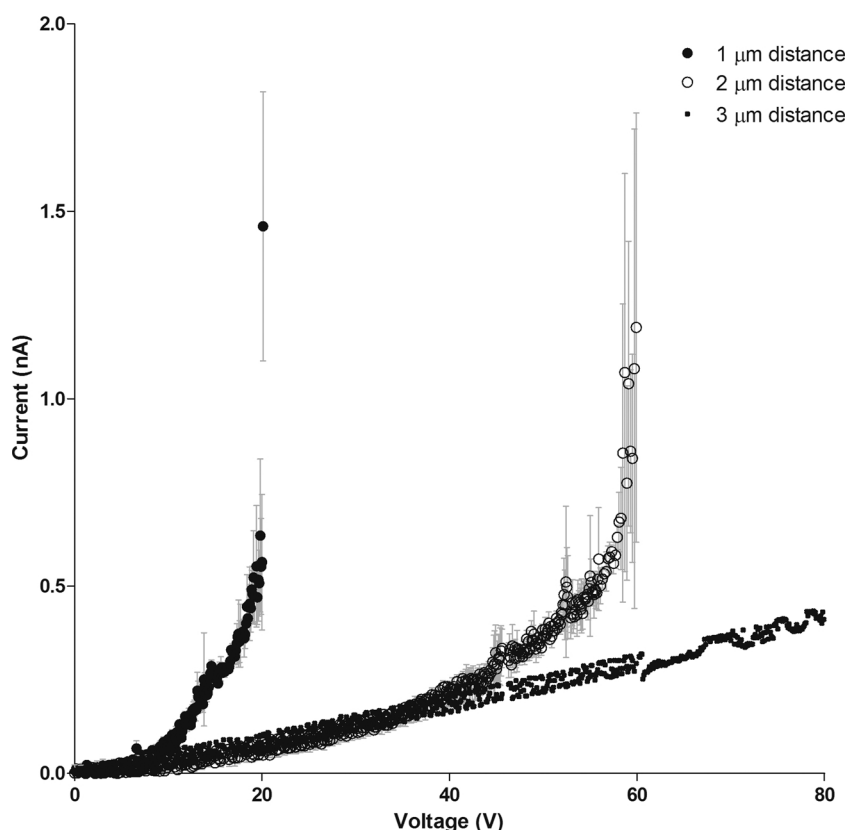
Fig. 3. Current-voltage curves measured in microreactors filled with *n*-hexane and with different electrode gaps.

in the patterned areas by wet etching in a solution of $KI:I_2:H_2O$ (4:1:40) for 1 min followed by a solution of chromium etchant (BASF) for 20 s. Both etch steps were followed by rinsing in demineralized water and spin drying. The flow channel was subsequently created by immersion in a 25 vol-% HF solution (BASF, 51151083) for 25 min, followed by rinsing in demineralized water and spin drying. The cross section of the obtained channel is 150 μm wide and 25 μm deep. The photoresist and the Au/Cr mask were removed using 99% nitric acid (UN2031 OM Group) and with a solution of $KI:I_2:H_2O$ (4:1:40) and a solution of chromium etchant (BASF), respectively. Access holes to the metallic electrodes were created via powder blasting [14].

After cleaning in piranha solution (3 parts 98% sulfuric acid, 1 part 30% hydrogen peroxide solution) for 30 min, the processed silicon and glass wafers were thermally bonded (Heraeus, temperature 600 °C for 1 h) and individual microreactors of 20 mm by 15 mm were cut out of the stack with a dicing machine (Disco DAD-321).

3.2. Field emission experiments in CFE microreactor

In the fabricated microreactors cold field emission was studied in *n*-hexane, which is an apolar aprotic solvent (*n*-hexane 95% from Sigma-Aldrich). Using a source measurement unit (Keithley, 2410) the required electrical field was generated by applying a negative potential to the cathode, with the anode grounded. Current-voltage curves were recorded via a custom made Labview program. The two electrodes were connected to the source measurement unit via spring connectors (MCS004, Mill Max), which ensure proper electrical contact between the microreactor and the rest of the setup. By using a Harvard pump (Harvard Apparatus, PHD 2000) and a 2.5 mL syringe (Hamilton Gastight) the solvent was flushed into and through the microdevice. Current-voltage measurements were done for continuous (from 1 to 10 μL/min) and stopped flow. Before and after each measurement ca. 100 μL of fresh solvent was flushed through the microreactor.

3.3. Chemical reaction in CFE microreactors

In order to prove the possibility of cold field emission for the generation of solvated electrons and their application in chemical synthesis, the microreactors were used for the partial reduction of anthracene. Solutions of 5 mM of anthracene (Sigma-Aldrich, 97%) in *n*-hexane (Sigma-Aldrich, 95%) or in *n*-hexane + 25 vol-% of ethanol (VWR 99%, 10009831000) were fed in continuous flow (1 μL/min) upon applying a constant current of 5 μA. For each electrode spacing a total of 1 mL of reactant was collected in a vial and analyzed with a GC–MS (Agilent Technologies, GC 7890A MS 5975C).

4. Results and discussion

4.1. Model results

The modeling results are graphically summarized in Fig. 2b) and c). The electric field is represented by a 2D field line plot in Fig. 2b). Clearly, the highest convergence of the field lines occurs at the tips of the triangular cathode, demonstrating the expected field enhancement. The 3D model (Fig. 2d) shows an arrow line plot of the electric field along the z-direction of the electrodes. This plot indicates that also in the direction perpendicular to the plane of the electrodes the field lines converge, which adds to the field emission enhancement. The electric field distribution between the electrodes is similar for different distances between the electrodes, the intensity of the electric field (for a fixed applied potential) scales inversely with the distance.

4.2. Electrical characterization

Scanning Electron Microscope (HR-SEM; Zeiss, Merlin) analysis of the metallic electrodes with micro tips on a silicon wafer before bonding revealed that the fabrication process was reproducible and that microtips with different electrode gap have similar geometry. An
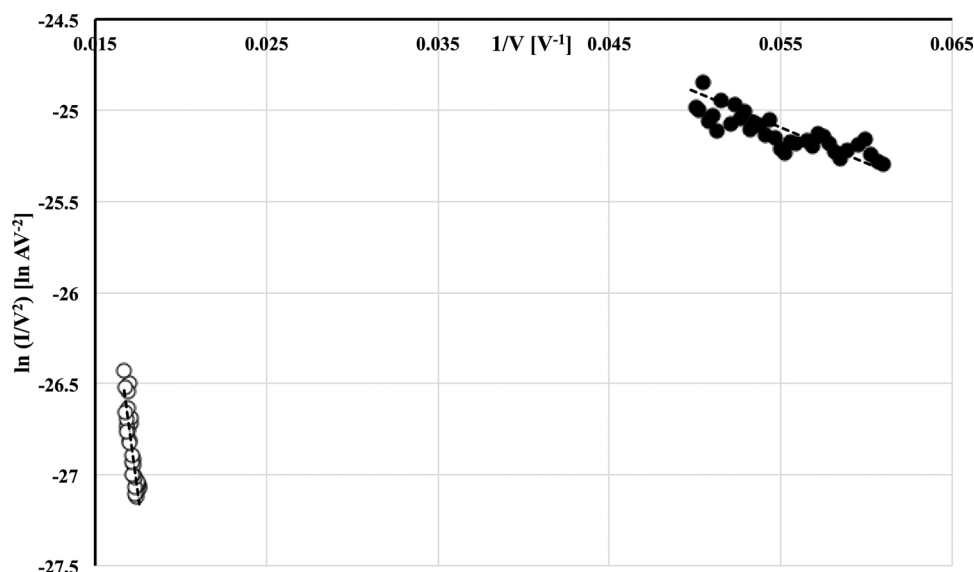
Fig. 4. Fowler-Nordheim plot for microreactors filled with *n*-hexane. Closed and open symbols: 1 μm and 2 μm tip-to-cathode distance, respectively.

example of a realized electrode pattern is shown in Fig. 1d. The radius of curvature of the tips, measured from SEM images of several tips, was found to be 350 ± 50 nm.

In Fig. 3 current-voltage curves, obtained by applying a negative potential to the cathode with the microtips, are shown for microreactors of which the flow channel is filled with *n*-hexane and with different distances between the electrodes. Electrical measurements were carried out at least three times in each of the different microreactors with different electrode gaps, and show very reproducible behavior, within experimental error. The observed exponential behavior is characteristic for cold field emission. In order to evaluate whether the measured data follow Fowler-Nordheim (F-N) tunneling theory for field electron emission [15], the measured data are re-plotted in F-N coordinates in Fig. 4. These plots demonstrate reasonable linearity for the cases with a gap of 1 or 2 μm, which suggests that field electron emission has occurred in the microreactor. For the 3 μm electrode distance, the reached electric field values were not high enough to establish whether true FN CFE occurs.

For further analysis of the current-voltage data, we will use the formulism given by Hong et al. [16]. For an array of emitter tips the following equation for the FN current is given:

$$I = n\alpha C_1 \phi^{-1} E^2 exp\{-C_2 \phi^{1.5}/E\} exp\{9.87/\sqrt{\phi}\} \tag{2}$$

where E, the electric field at the tip surface, is defined as $E = \beta V$, with β (cm^{-1}) a geometry factor that converts the applied voltage to the electric field at the surface of the tip. This is quite similar to what has been termed an enhancement factor in some publications, with the understanding that in Hong's formulism the gap between emitter tip and cathode is implicit in the parameter β. C_1 and C_2 are constants, with respective values of $1.4\ 10^{-6}$ eV A V^{-2} and $6.53\ 10^7$ V $eV^{-3/2}$ cm^{-1}. n is the number of emitters in the array (600 in our case), and α (cm^{-2}) the emitting area per in tip, assuming that all tips in the array emit equally.

Φ is the potential barrier that has to be overcome in order to emit an electron from the Pt microstructured cathode into the surrounding medium. In Eq. (2), which was developed for CFE in vacuum, it would therefore be equal to the common work function of Pt. As was discussed in our previous report [11], the barrier will be reduced by the final energy state of the electrons when they become solvated in the dielectric liquid hexane. This energy reduction is reported to be 0.02–0.09 eV [17]. As was noted by Gossenberger et al., the experimental values of the work function of clean platinum generally do not agree well and are in the range of 5.6 eV–6.1 eV. We decided therefore

to take Gossenberger's calculated value of 5.71 eV for Pt (111) [18], since our sputtered metal films typically have (111) texture [19]. The actual work function will thus be reduced to 5.65 eV if we subtract the average value of the electron immersion energy range in hexane given above. A second correction factor that might be relevant is the dielectric constant of the liquid medium. In the derivation of the Fowler-Nordheim Eq. (2), the effect of image forces on the tunneling barrier is largely neglected, because it is typically of the order of one percent [20]. These image forces would change somewhat by going from vacuum to liquid hexane, but since the dielectric constant of hexane is 1.89 and therefore of the same order of magnitude as that of vacuum, the effect remains negligible.

By plotting the emission current of Eq. (2) in FN coordinates, as is done in Fig. 4, a straight line results with a slope P and an intercept Q, given by [16]:

$$P = -6.53 \cdot 10^7 \left\{ \frac{\phi^{3/2}}{\beta} \right\} \tag{3}$$

$$Q = ln \left\{ 1.4 \cdot 10^{-6} n\alpha \frac{\beta^2}{\phi} exp\left(\frac{9.87}{\sqrt{\phi}} \right) \right\} \tag{4}$$

Applying these equations on the data in Fig. 4 results in the values of α and β in Table 1. In comparison to the values calculated by Hong et al. for a number of different field emitter structures with reported tip radii of 25–50 nm [16], our number for the 1 μm gap for β is 1 to 2 orders of magnitude higher, and for α at least 5 orders of magnitude lower. Our values for the 2 μm gap are in reasonable agreement with Hong's numbers, although our α value is on the low side.

From the β values in Table 1, a field enhancement factor at the emitter tips can be derived by multiplying β by the gap distance, which leads to values of 22.3 and 2.48 for the 1 and 2 μm gap, respectively. If we follow Hong et al., who take the field enhancement factor as the

Table 1
Fowler-Nordheim analysis of CFE measurements.

Electrode gap μm	P V ln (A V^{-2})	Q ln (A V^{-2})	α cm^{-2}	β cm^{-1}
1	−39.3	−22.9	$2.41\ 10^{-23}$	$2.23\ 10^7$
2	−709	−14.7	$2.84\ 10^{-17}$	$1.24\ 10^6$
1 [a]	−8.20	−14.3	$5.83\ 10^{-20}$	$1.07\ 10^8$

[a] Based on data voor 5 mM anthracene dissolved in a 1:3 mixture of ethanol:hexane (see Section 4.3 and Fig. 5).

product of β and the sum of the gap and the tip height (and thus compare the tip configuration with a flat electrode at a gap distance at the base of the tips), we arrive at enhancement factors of 245 and 15, respectively.

In a first approximation the emitting area per tip in our case is equal to $\pi R h$, with R the radius of curvature of the tip, as measured from SEM images (see Fig. 1d; R has a measured value of 350 nm) and h the thickness of the anode layer (110 nm, being the total thickness of the Pt/Ta layer). This leads to a value of $1.2 \, 10^{-9} \, cm^{-2}$, which is several orders of magnitude larger than the values of α in Table 1. Qualitatively this is in agreement with the findings of Hong et al. [16], who also arrive at the conclusion that FN analysis implicates extremely small emitting area, much smaller than the real, measured tip radius. They attribute this to interactions between neighbouring emitters which enhance the electrical field around the tips, but do not exclude the enhancing effect of microprotrusions with very small radius of curvature. We were not able to determine the radius of curvature of the edges of the metal pattern, which is defined by the photoresist pattern quality, which most likely is smaller than the in-plane radius of the tips. Furthermore, we do not exclude that very sharp Pt protrusions have remained at the metal pattern edges after the photoresist lift-off process ("lift-off ears" [21]). Nevertheless, even such much smaller emitter tips cannot explain the extremely small emitting areas derived in Table 1.

A final observation worth mentioning is that for a variation of the hexane flow rate in the range 1 to 10 μL/min for a specific electrode distance no significant difference was found in the current-voltage curves. This is expected, since Such a flow variation (and its associated residence time variation) can be expected to have an effect on the outcome of the chemical experiments to be discussed below.

4.3. Chemical reactions in CFE microreactors

GC analysis of solutions obtained after exposure to field electron emission in the microreactor devices indicates that pure n-hexane is inert during the partial reduction of anthracene. The density of emission points on the electrodes, the current that passes through the liquid, the absence or presence of a proton donor in the solution and the geometry of the microfluidic device (in our case the electrodes are placed at the bottom of the flow channel) are all relevant factors for the reduction reaction. A proton donor is necessary to continue the reduction after the formation of the anthracene radical anion, and alcohols are commonly added for this purpose. Here, a 5 mM solution of anthracene in n-hexane containing 25%vol of ethanol was loaded into microreactors with electrode gaps of 1, 3, 5, 10 and 20 μm. First, similar current-voltage curves as in Fig. 3 were measured, to determine if field electron emission also occurs in this mixture. It was found that, compared to pure hexane, the currents in this case are 2–3 orders of magnitude, which we attribute to the polar compound ethanol. The result for an electrode gap of 1 μm is shown, plotted in Fowler-Nordheim coordinates, in Fig. 5. The fitting parameters for the obtained curve are given in Table 1.

Also here, we neglected the image force contribution on the tunneling barrier, which is influenced by the dielectric constant. Even though the dielectric permittivity for ethanol is relatively high (24.5), that of the 1:3 mixture in n-hexane is probably ca. 2–3 and of the same order of pure n-hexane, an assumption that we base on the measured permitivity values of mixture series of 1-pentanol, 1-hexanol and 1-heptanol with n-hexane [22]. Furthermore, because of a lack of literature data, we used the same correction as before for the work function of platinum. Note that the value of β in Table 1 is about a factor 5 higher than in the case of pure hexane, which can be attributed to local electric field line intensification because the mixture has a higher dielectric permittivity than pure hexane. The observation that the value of α (emitting area) is about 3 orders of magnitude higher in the mixture than in pure hexane could have a similar cause: possibly the field lines originating from further away from the tip, see Fig. 2(c), are

focused such that the effective emitting area becomes larger. This effect needs a closer investigation, which is out of the scope of this publication.

For the chemical reactions in the solution mentioned above, either a constant current of 5 μA was applied, or in cases where such a current could not be obtained, a maximum voltage of 80 V was maintained in order to avoid electrical breakdown of the SiO_2 layer beneath the electrodes. The results are shown in Table 2. As can be seen, conversions are quite low, and the expected reduction product, 9,10-dihydroanthracene, is not detected, irrespective of the conditions. We attribute this result to two effects: i) the low density of emitters present in the microreactor (600 microtips over a length of 6 mm), giving a relatively low solvated electron density in the solution, and ii) the oxidation of any formed 9,10-dihydroanthracene at the platinum anode, to anthracene, or to other oxidation products. The latter is supported by previous reports that the electroreduction of anthracene to 9,10-dihydroanthracene is reversible: Gagyi-Pálffy et al. [23], who performed electrochemical reduction of anthracene, mention that in an undivided electrochemical cell, the hydrogenation of anthracene is hindered by competitive reactions, being the already mentioned oxidation of the 9,10-dihydroanthracene back to anthracene and the oxidation of this compound to 9,10-dihydroxyanthracene and anthraquinone.

The fact that in our case the platinum counter electrode has a significant oxidative effect on the product formation follows from the data in Table 2. The GC–MS analysis of reacted solutions for various gaps and a flow of 1 μL/min shows the formation of two main substances, 9-ethyl-10-methyl-9,10-dihydroanthracene (product A) and 9-ethyl-anthrone (product B). The assignments are based on the mass spectra of the different fragments obtained by GC–MS, which were run through a mass spectrometry database to obtain the most likely corresponding compound(s). Note that with these MS data, it is not possible to determine the substitution position of the ethyl and methyl groups, therefore we have opted for the most probable positions 9 and 10, where originally the extra electron(s) from the emission process are expected to be attached. Other techniques, such as NMR are needed to give a definitive answer about the exact molecular structure, we did not perform such an analyis here because of the very limited product yield, in the μL-range.

Clearly, the product 9-ethyl-10-methyl-9,10-dihydroanthracene (product A in Table 2) must have formed by a reaction of anthracene or 9,10-dihydroanthracene with ethyl and methyl cations or radicals, and these can only originate from the ethanol. Most likely, instead of the desired proton addition, an ethyl group was added to the 9 position of an anthracene radical anion that was first formed by the addition of a solvated electron to the anthracene aromatic ring. A possible mechanism for this reaction is that the anthracene radical anion performs a nucleophilic substitution on ethanol, by which a hydroxide ion is released. It is not unlikely that this, or a related process, occurs at the platinum anode surface, a hypothesis that is in line with the presence of the methyl substituent. Methyl groups are known to form on the surface of platinum electrodes, due to dissociative adsorption of ethanol [24]. Therefore, we conclude that product A has been formed by electrooxidation of 9,10-dihydroanthracene on the platinum anode. Note that the product 10-methylanthracene-9-carboxaldehyde has the same molecular mass as product A, however, its mass spectrum [25] does not match the measured data. Along the same lines we hypothesize that product B, 9-ethyl-10-anthrone, has been formed by a mechanism that passes through an intermediate state in which the ethanol molecule bridges the central ring of the anthracene radical anion, and possibly this happens at the platinum electrode. More detailed studies are needed to make definitive conclusions about the reaction mechanism, e.g. by applying the platinum anode on an ATR crystal integrated in a microreactor [26].

Due to the relatively low conversions in Table 2, it is not possible to draw convincing conclusions about the effect of electrode gap on the chemical processes. For gaps below 5 μm, it was possible to perform
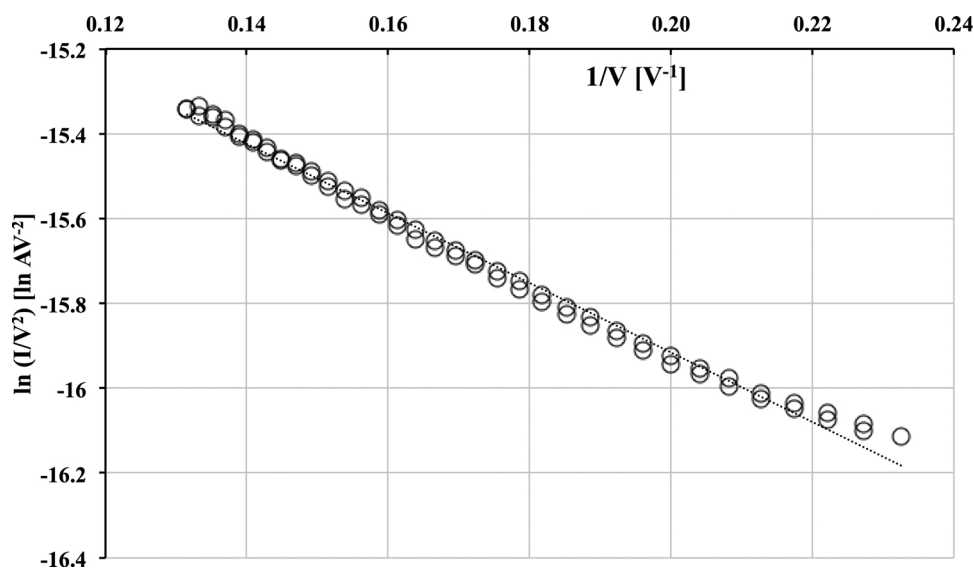
Fig. 5. Fowler-Nordheim plot for a microreactor with a 1 μm electrode gap, filled with a solution of 5 mM anthracene in a 1:3 mixture of ethanol: *n*-hexane.

Table 2

Reaction products based on GC–MS analysis, for field electron emission into solutions containing 5 mM anthracene in hexane with 25 vol% ethanol.

Current μA	Electrode gap μm	Conversion (%)	Product A [a] (%)	Product B [b] (%)
5	1	5.6	2.5	3.1
5	3	4.0	1.7	2.3
5	5	4.6	1.2	2.4
3	10	2.0	0.6	1.5
1	20	0	0	0

[a] Product A, most likely this is cis or trans 9-ethyl-10-methyl-9,10-dihydroanthracene. MS data (m/z, intensity): 17.000,197.000; 18.100,796.000; 28.000,619.000; 31.900,366.000; 165.000,286.000; 176.000,137.000; 178.000,569.000; 179.000,458.000; 192.900,710.000; 194.100,542.000; 195.100,392.000; 222.100,732.000; 223.000,160.000.

[b] Product B, 9-ethyl-10-anthrone: MS data (m/z, intensity) 17.000,260.000; 18.000,809.000; 28.000,557.000; 31.900,285.000; 82.800,118.000; 87.800,113.000; 138.900,187.000; 150.100,118.000; 163.000,531.000; 164.000,408.000; 165.000,2064.000; 166.000,240.000; 176.100,173.000; 178.000,137.000; 193.000,3759.000; 194.000,1668.000; 194.900,201.000; 206.900,119.000; 207.900,103.000; 222.000,1633.000; 223.100,286.000.

experiments at the same recorded current, without a significant trend in conversion or product selectivity. More work is needed to investigate this parameter, although the priority, for effective partial reduction of polycyclic aromatic compounds, should be to eliminate the oxidation pathways, which might perhaps be achieved with a different anode material, or better still, by constructing a microreactor with divided compartments for cathode electron emission and anode electron collection. To increase the reduction yield, we envision a cathode with a larger density of emitter tips, e.g. by implementing carbon nanotubes [27].

5. Conclusions

The proposed study confirms the possibility to generate cold field emission in pure *n*-hexane and a *n*-hexane/ethanol mixture with dissolved anthracene, by using a potential of a few tens of Volts on electrodes with small electrode gaps and with sharp tips to enhance the electric field between the electrodes. Field emission in pure *n*-hexane with the proposed microreactor does not directly reduce aromatic hydrocarbons, for that the addition of a proton donor is necessary, for which ethanol was chosen. In this way, in solutions of *n*-hexane and ethanol a mixture of products identified as 9-ethyl-10-methyl-9,10-dihydroanthracene and 9-ethyl-10-anthrone are formed, which are

thought to be due to electrochemical degradation of the alcohol on the platinum counterelectrode, and reaction of the degradation products with the desired reduction product 9,10-dihydroanthracene. The knowledge acquired in this work will be useful for future microreactor devices for the partial reduction of polycyclic aromatic hydrocarbons based on cold field emission to inject electrons in liquids, however, an approach has to be found to avoid the oxidation at the counterelectrode, which possibly could be achieved by designing a microreactor with divided anode and cathode compartments.

Acknowledgements

References

[1] M. Chiesa, M.C. Paganini, E. Giacomello, D.M. Murphy, C. Di Valentin, G. Pacchioni, Excess electrons stabilized on ionic oxide surfaces, Acc. Chem. Res. 39 (2006) 861–867, http://dx.doi.org/10.1021/ar068144r.

[2] W. Weyl, Uber metallammonium-verbindungen, Ann. Phys. 197 (1864) 601–612, http://dx.doi.org/10.1002/andp.18641970407.

[3] B. Abel, U. Buck, A.L. Sobolewski, W. Domcke, On the nature and signatures of the solvated electron in water, Phys. Chem. Chem. Phys. 14 (2012) 22–34, http://dx.doi.org/10.1039/C1CP21803D.

[4] A.J. Birch, Reduction by dissolving metals. Part 1, J. Chem. Soc. (1944) 430–436, http://dx.doi.org/10.1039/JR9440000430.

[5] H.W. Sternberg, R. Markby, I. Wender, Electrochemical reduction of benzene ring, J. Electrochem. Soc. 110 (1963) 425–429, http://dx.doi.org/10.1149/1.2425779.

[6] N. Na, Y. Xia, Z. Zhu, X. Zhang, R.G. Cooks, Birch reduction of benzene in a low-temperature plasma, Angew. Chem. Int. Ed. 48 (2009) 2017–2019, http://dx.doi.org/10.1002/anie.200805256.

[7] E. Kariv-Miller, K.E. Swenson, D. Zemach, Cathodic Birch reduction of methoxyaromatics and steroids in aqueous solution, J. Org. Chem. 48 (1983) 4210–4214, http://dx.doi.org/10.1021/jo00171a011.

[8] B. Halpern, R. Gomer, Field emission in liquids, J. Chem. Phys. 51 (1969) 1031–1047, http://dx.doi.org/10.1063/1.1672102.

[9] K. Dotoku, H. Yamada, S. Sakamoto, S. Noda, H. Yoshida, Field emission into nonpolar organic liquids, J. Chem. Phys. 69 (1978) 1121–1125, http://dx.doi.org/10.1063/1.436689.

[10] A.G. Krivenko, N.S. Komarova, N.P. Piven, Electrochemical generation of solvated electrons from nanostructured carbon, Electrochem. Commun. 9 (2007) 2364–2369, http://dx.doi.org/10.1016/j.elecom.2007.07.004.

[11] A. Agiral, H.B. Eral, D. van den Ende, J.G.E. Gardeniers, Charge injection from carbon nanofibers into a dielectric liquid under ambient conditions, IEEE Trans. Electron. Devices 58 (2011) 3514–3517, http://dx.doi.org/10.1109/TED.2011.2160947.

[12] D.J. Griffiths, Introduction to Electrodynamics, 3rd ed., Prentice hall, 1999.

[13] I.S. Grant, W.R. Philips, Electromagnetism, Manchester Physics Series, 2nd ed., John Willey & Sons, 1990.

[14] H. Wensink, H.V. Jansen, J.W. Berenschot, M.C. Elwenspoek, Mask materials for powder blasting, J. Micromech. Microeng. 10 (2000) 175–180, http://dx.doi.org/10.1088/0960-1317/10/2/313.

[15] R.H. Fowler, L. Nordheim, Electron emission in intense electric field, Proc. R. Soc. A 119 (1928) 173–181, http://dx.doi.org/10.1098/rspa.1928.0091.

[16] D. Hong, M. Aslam, M. Feldmann, M. Olinger, Simulations of fabricated field emitter structures, J. Vac. Sci. Technol. B 12 (1994) 764–769, http://dx.doi.org/10.1116/1.587387.

[17] R.A. Holroyd, M. Allen, Energy of excess electrons in nonpolar liquids by photo-electric work function measurements, J. Chem. Phys. 54 (1971) 5014–5021, http://dx.doi.org/10.1063/1.1674791.

[18] F. Gossenberger, T. Roman, K. Forster-Tonigold, A. Groß, Change of the work function of platinum electrodes induced by halide adsorption, Beilstein J. Nanotechnol. 5 (2014) 152–161, http://dx.doi.org/10.3762/bjnano.5.15.

[19] R.M. Tiggelaar, A.W. Groenland, R.G.P. Sanders, J.G.E. Gardeniers, Stability of thin platinum films implemented in high-temperature microdevices, Sens. Actuators, A 152 (2009) 39–47, http://dx.doi.org/10.1016/j.sna.2009.03.017.

[20] M. Lenzlinger, E.H. Snow, FowlerNordheim tunneling into thermally grown SiO₂, J. Appl. Phys. 40 (1969) 278–283, http://dx.doi.org/10.1063/1.1657043.

[21] M. Dimaki, M. Vergani, A. Heiskanen, D. Kwasny, L. Sasso, M. Carminati, J.A. Gerrard, J. Emneus, W.E. Svendsen, A compact microelectrode array chip with multiple measuring sites for electrochemical applications, Sensors 14 (2014)

9505–9521, http://dx.doi.org/10.3390/s140609505.

[22] T.P. Iglesias, J.L. Legido, S.M. Pereira, B. de Cominges, M.I. Paz Andrade, Relative permittivities and refractive indices on mixing for (n-hexane + 1-pentanol, or 1-hexanol, or 1-heptanol) at T = 298.15 K, J. Chem. Thermodyn. 32 (2000) 923–930, http://dx.doi.org/10.1006/jcht.2000.0661.

[23] E. Gagyi-Pálffy, P. Starzewski, A. Labani, A. Fontana, Electrochemical reduction of polyaromatic compounds, J. Appl. Electrochem. 24 (1994) 337–343, http://dx.doi.org/10.1007/BF00242063.

[24] A. Bach Delpeuch, F. Maillard, M. Chatenet, P. Soudant, C. Cremers, Ethanol oxidation reaction (EOR) investigation on Pt/C, Rh/C, and Pt-based bi- and tri-metallic electrocatalysts: a DEMS and in situ FTIR study, Appl. Cat. B 181 (2016) 672–680, http://dx.doi.org/10.1016/j.apcatb.2015.08.041.

[25] Permanent link for properties of 10-Methylanthracene-9-carboxaldehyde: http://webbook.nist.gov/cgi/inchi/InChI%3D1S/C16H12O/c1-11-12-6-2-4-8-14%2812%2916%2810-17%2915-9-5-3-7-13%2811%2915/h2-10H%2C1H3.

[26] A. Susarrey-Arce, R.M. Tiggelaar, M. Morassutto, J. Geerlings, R.G.P. Sanders, B. Geerdink, S. Schlautmann, L. Lefferts, A. van Houselt, J.G.E. Gardeniers, A new ATR-IR microreactor to study electric field driven processes, Sens. Actuators, B 220 (2015) 13–21, http://dx.doi.org/10.1016/j.snb.2015.05.025.

[27] M. Morassutto, R.M. Tiggelaar, M. Smithers, J.G.E. Gardeniers, Vertically aligned carbon nanotube field emitter arrays with Ohmic base contact to silicon by Fe-catalyzed chemical vapor deposition, Mater. Today Commun. 7 (2016) 89–100, http://dx.doi.org/10.1016/j.mtcomm.2016.04.007.